A microfluidic device to apply shear stresses to polarizing ciliated airway epithelium using air flow

Dennis Trieu,[1] Thomas K. Waddell,[1,2,3,a)] and Alison P. McGuigan[1,4,a)]
[1]*Institute of Biomaterials and Biomedical Engineering, University of Toronto, 200 College St., Toronto, Ontario M5S 3E5, Canada*
[2]*Latner Thoracic Surgery Research Laboratories and the McEwen Centre for Regenerative Medicine, Toronto General Hospital, Toronto, Ontario M5G 2C4, Canada*
[3]*Institute of Medical Science, University of Toronto, 200 College St., Toronto, Ontario M5S 3E5, Canada*
[4] *Department of Chemical Engineering and Applied Chemistry, University of Toronto, 200 College St., Toronto, Ontario M5S 3E5, Canada*

(Received 16 July 2014; accepted 5 November 2014; published online 14 November 2014)

Organization of airway epithelium determines ciliary beat direction and coordination for proper mucociliary clearance. Fluidic shear stresses have the potential to influence ciliary organization. Here, an *in vitro* fluidic flow system was developed for inducing long-term airflow shear stresses on airway epithelium with a view to influencing epithelial organization. Our system consists of a fluidic device for cell culture, integrated into a humidified airflow circuit. The fluidic device has a modular design and is made from a combination of polystyrene and adhesive components incorporated into a 6-well filter membrane insert. We demonstrate the system operates within physiologically relevant shear and pressure ranges and estimate the shear stress exerted on the epithelial cell layer as a result of air flow using a computational model. For both the bronchial epithelial cell line BEAS2B and primary human tracheal airway epithelial cells, we demonstrate that cells remain viable within the device when exposed to airflow for 24 h and that normal differentiation and cilia formation occurs. Furthermore, we demonstrate the utility of our device for exploring the impact of exposing cells to airflow: our tool enables quantification of cytoskeletal organization, and is compatible with *in situ* bead assays to assess the orientation of cilia beating.
[http://dx.doi.org/10.1063/1.4901930]

I. INTRODUCTION

Tracheal resection and reconstruction is the gold standard to repair short injuries caused by disease and physical damage; however, there are currently no reliable clinical treatments for reconstructing large segments of injured trachea.[1] In recent clinical trials, decellularized tracheal allografts and tissue engineered scaffolds have been implanted in patients with successful results to treat large tracheal defects.[2–4] While the results of these trials suggest that scaffolds functioned as a stable tube for airflow transfer, recipients were susceptible to recurrent infections and mucous impaction after the surgery, which may be in part due to incorrect organization and hence dysfunction of the airway epithelium.[5,6]

Airway epithelium is comprised of a pseudostratified monolayer layer of columnar epithelial cells on top of a basement membrane. Airway epithelial cells are apicobasally polarized, such that there is an unequal distribution and organization of cellular components in the top (apical) region of the cell compared to the bottom (basal) region of the cell.[7] Apicobasal

[a)]Authors to whom correspondence should be addressed. Electronic addresses: alison.mcguigan@utoronto.ca and tom.waddell@uhn.ca

polarization is induced by a difference of the microenvironments above and below the cell. In airway epithelium, this difference is provided by the presence of air and airway surface liquid on the apical surface, while the basal surface of the cell is attached to the basement membrane. In airway epithelium, apicobasal polarization is essential for the formation of cilia. Cilia are microtubule-based structures that protrude through the apical surface of the cell membrane and are attached to the cytoskeleton through actin and microtubule networks that enable mucous movement within the airways.[8,9] Coordinated beating of cilia in the airway is critical to remove mucus and prevent mucous compaction.[6] Strategies to generate correctly organized epithelium in which cilia beating is coordinated are therefore critical for improving clinical success with engineered tracheal grafts.

The gold standard for generating polarized airway epithelium *in vitro* is by culturing the cells in air-liquid interface culture.[10] Specifically, airway epithelial basal cells are grown on a porous filter membrane to confluence with specialized medium in the apical and basal compartments. Once the cells have formed a confluent monolayer, the medium in the apical compartment is removed to generate an air interface on the apical surface of the cells and the basal media compartment is replaced with specialized differentiation media.[11] The epithelium then differentiates and cilia formation occurs over a period of 14 to 45 days of air-liquid interface culture. While this method allows the generation of apicobasally polarized epithelium with functional cilia on the apical surface, these cilia lack tissue-level coordination and do not beat synchronously in one coordinated direction.[11–13] Recent studies, using explanted tissue, suggest that shear stresses from flowing liquids, applied in appropriate time windows, can orient the direction of cilia beating in *Xenopus*[14] and mouse ependymal epithelial cell models[15] to produce global coordination. In airway epithelium however, application of fluid flow is undesirable because an air-liquid interface is necessary for proper maturation of airway epithelial cells and submerged cultures inhibit *in-vitro* differentiation.[16] Since a major source of fluidic shear stress in the airways comes from the movement of air during inhalation and exhalation, the application of shear stress via air flow on the differentiating airway epithelium is an attractive strategy to potentially generate global cilia coordination. Due to technical limitations however, to date only short exposures to shear from airflow of less than one hour in duration have been studied.

Only a few studies have explored the effects of controlled airflow shear stress on airway epithelial cells.[13,17,18] In these studies cells are exposed to airflow forces via airflow shear stresses or cyclic compressive pressure in custom-built filter membrane wells that are placed inside an airflow exposure chamber. The use of cyclic compressive pressure causes intermittent airflow shear stresses but, at least in the studies reported, these shear stresses have not been accurately controlled.[13] Furthermore, current systems that are capable of applying controlled shear stresses have large supporting equipment making them unsuitable to be placed inside a controlled incubator for long-term culture.[17,18] These limitations have prevented the ability to apply controlled long-term airflow shear stresses on primary airway epithelial cells to understand the impact of airflow on cell polarization.

Here, we describe a device that allows the application of controlled shear levels via air flow on airway epithelial cells under the air-liquid interface culture conditions required to produce apicobasal polarization. Using a modular approach, we assembled a device with an open channel that could be enclosed at the desired time point to apply air flow, and in which cells could be cultured on a filter membrane to enable air-liquid interface. The device can be easily fabricated, utilizes commercially available filter membrane inserts that are used in standard air-liquid interface culture, and allows application of controlled shear levels via air flow. We demonstrate the system operates within physiologically relevant shear and pressure ranges and estimate the shear stress exerted on the epithelial cell layer as a result of air flow using a computational model. For both the bronchial epithelial cell line BEAS2B and primary Human Tracheal Epithelial Cells (HTEC), we demonstrate that cells remain viable within the device when exposed to airflow for 24 h and that normal differential formation of cilia occurs. Furthermore, we demonstrate that our device is compatible with standard assays to quantify cytoskeletal organization and cilia beating.

II. MATERIALS AND METHODS

A. Device fabrication and assembly

Polystyrene discs for the device were fabricated by end milling a 0.830 mm polystyrene sheet with a computer numerical control desktop milling kit (Shapeoko combined with GRBLShield) interfaced with computer numerical control software (UniversalGCodeSender). Computer-aided design models were designed and translated to G-Code for milling operations using computer-aided manufacturing software (CamBam Plus).

Adhesives transfer tape discs were fabricated by die cutting adhesive transfer tapes using a desktop cutting machine (Cricut Mini). Inlet and outlet connections were made by drilling 0.85 mm pilot holes in the lid layer and screwing in 18 G stainless steel tubing connectors threaded with a #0–80 thread. Stainless steel tubing connectors were made by cutting off the ends of 18 G needles and threading the ends with a #0–80 die.[19] 1.05 mm inner diameter polyethylene tubing (Intramedic, Becton Dickinson) was twisted onto the stainless steel tubing connectors which provided a leakage free connection. Polystyrene discs were attached to a porous polyester membrane (Costar Transwell 0.4 μm Permeable Support) using the silicone adhesive transfer tape. The polystyrene and adhesive transfer tape discs were 24 mm in diameter and the slots were 10 mm long, 1 mm high, and 4 mm wide.

B. Fluidic system design

Our fluidic system is comprised of three sub-systems: an airflow conditioning system, a fluidic device where cells are grown and cultured, and a data acquisition system that monitors the airflow rates being applied over the cells. System components were sterilized by UV irradiation, bathing components in 70% ethanol, and rinsing the ethanol with sterile MilliQ water. An overview of the components and operation of the fluidic system is shown in Figure 1.

1. Air-conditioning sub-system

Heated incubator air was sterilized using a 0.2 μm syringe filter (VWR Sterile Acetate Syringe Filter, 28145–477) and re-circulated throughout the fluidic system using a micro air pump (Sensidyne Series A Plus). The filtered air was combined with sterile phosphate buffered saline (PBS) at a T-valve. The air-water mixture was pushed through two reservoirs filled with sterile PBS to further humidify the airflow. Large water particles in the air-water mixture that could clog the system were separated using a condenser. The conditioned airflow rate was controlled by changing the resistance of the airflow through a needle flow splitter valve.

2. Airflow monitoring sub-system

Volumetric airflow rates were measured using a microelectromechanical airflow sensor (Omron D6F-P) at the output of the fluidic device through a data acquisition system and software (Arduino Mega 2560 and National Instrument's Labview 2011). To ensure that the airflow rate measured by the airflow sensor was correct, the sensor calibration was validated using a syringe pump (PHD 2000, Harvard apparatus) containing a 60 ml syringe that applied known airflow rates. The maximum airflow shear stresses being applied on the cells was calculated from the volumetric airflow rates and geometric dimensions of the rectangular channel using the following equation for laminar flow as described by Young *et al.*:[20]

$$\tau_w = \frac{2\mu Q}{wh^2}\left(1+\frac{1}{m}\right) * (n+1), \tag{1}$$

where τ_w is the wall shear stress, μ is the dynamic viscosity of humid air, Q is the volumetric flow rate, w is the width of the channel, h is the height of the channel, and m and n are empirical constants.

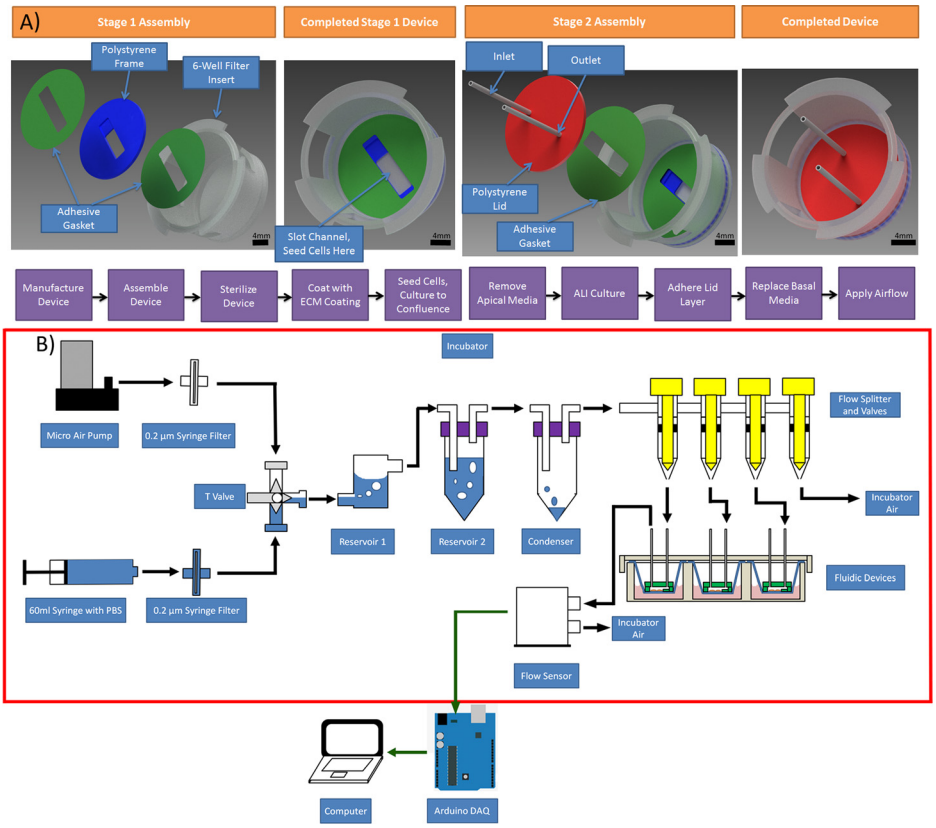

FIG. 1. Fluidic system design. (a) Device design and fabrication and (b) airflow system design

C. Pressure testing and computational fluidic dynamics modelling

To examine the theoretical distributions of shear stresses caused by airflow, the device was modelled using Autodesk CFD Simulation 2014. The analysis was modelled using an incompressible transient laminar Navier-Stokes model. The laminar model was chosen because of the low Reynolds numbers present in the system. The finite element model was a simplified model based on the air-fluid domains only with rigid and immobile boundary walls. The model is comprised of the air-fluid domain within the device channel and attached tubing, which is shown in Figure 1 of the supplementary material.[43] The air in the inlet tubing was modelled as a humid air-fluid domain with a diameter varying from 0.838 to 3.06 mm and a length of a 92.5 mm. The tubing model is based on the actual tubing utilized in the system to produce a more representative airflow profile. The air in the outlet tubing was modelled as an air-fluid domain with 0.838 to 3.06 mm in diameter and 229 mm in length with a large 100 mm × 100 mm × 100 mm cube at the end of the outlet to simulate the air exiting to the incubator. The inlet and outlet air-fluid domains were meshed with a 1.6 mm length scale triangular mesh, while the air-fluid domain in the channel was modelled with a 0.1 mm length scale triangular mesh. In total, the model was comprised of 69 292 triangular mesh elements.

The model was setup with transient boundary conditions at the inlet tube with fluctuating air flow rates normal to the inlet tube surface, while the surfaces of the outlet box were set as static atmospheric pressure. The varying sinusoidal boundary conditions at the inlet, which can be seen in Figure 2 of the supplementary material,[43] were obtained from experimental measurements of air flow and pressure from the air pump. The transient solver was set with a time step size of 0.1 s with 10 inner iterations per time step and ran for 300 time steps. These settings were based upon convergence criteria to produce a reliable simulation. Convergence was considered for each time step when the average airflow rate and pressure values were less than 1%

different from the previous inner iteration. Convergence for the time length of the simulation was considered when the average pressure and airflow rate were less than 1% different from the previous sinusoidal cycle.

D. Airway epithelial cell culture

In this study, the human BEAS-2B cell line and primary HTEC are used for testing. BEAS-2B is an immortalized bronchial epithelial cell line and was used for initial testing because they are straightforward to culture. These cells however do not adequately behave like upper airway cells as they do not differentiate into multiciliated cells and they have poor mucociliary function.[21,22] We therefore also used HTEC in the system which, although harder to culture, has the capability to differentiate into goblet, club, basal, and ciliated cells[23] and HTEC grown at air-liquid interface culture have been shown to closely resemble the *in vivo* transcriptome.[24] The HTEC used in our study were primary tracheobronchial epithelial cells isolated from healthy lung transplant donors at the University Health Network (Toronto, Canada) and were a gift from Dr. Nadeem Moghal. HTEC provided a better representation of airway cells *in vivo*. HTEC cells received were screened for basal cell markers P63+, K5, and K14 since basal cells are thought to be the progenitor cell of airway epithelium and have the capability to differentiate into other airway cell types.[25]

BEAS-2B were cultured in DMEM/F12 medium containing 10% fetal bovine serum, 1% pencillin, 1% streptomycin. Passage zero HTEC was cultured in flasks coated with 60 μg/ml PureCol collagen and 0.1 M hydrochloric acid. Cells were grown using basal epithelial growth medium (Lonza Clonetics) until they are 80% confluent before passaging. The cells were expanded and passaged twice, with the cells being seeded in the devices on the second passage. Differentiation capability is highly dependent on the passage number of the HTEC. HTEC differentiation studies have shown that up to 50% of the apical surface cells can differentiate into multiciliated cells in passage 0 to passage 2 cells, while cells that have undergone more cell passages have significantly reduced multiciliated cell differentiation capability.[23] Cells were therefore all used at passage two.

BEAS-2B and HTEC were seeded into the apical slot of the device that was previously coated with 100 μg/ml PureCol Collagen (Advanced Biomatrix) and 25 μg/ml stabilized fibronectin (Biomedical Technologies Inc.) at 200 000 cells/cm^2 in an 80 μl droplet. After 3 h, the droplet was aspirated out and the apical and basal chambers were filled with media for long-term culture. Air-liquid interface culture was induced by aspirating out the media in both chambers and only refilling the basal chamber. For BEAS-2B cells, air-liquid interface was induced after 2 days of liquid-liquid culture. BEAS-2B were grown in the same BEAS-2B medium as previously described. For HTEC, air-liquid interface was induced after 3 h of liquid-liquid culture. Cells were cultured in B-ALI Medium (Lonza Clonetics) during air-liquid interface culture. A fresh batch of media with B-ALI inducer media supplement was made up prior to each medium change. For both BEAS2B and HTEC, medium in the basal compartment was changed every other day and any liquids found in the apical chamber were aspirated out. The liquids in the apical chamber comprised of any airway surface liquid generated by the cells. This airway surface liquid hydrates and protects airway epithelium and is expected to be present in functioning airway epithelium.[26,27]

E. Flow experiments

On the day before airflow was to be applied, the lid layer was adhered to the frame layer creating an enclosed channel. The basal media was also changed. Before applying airflow, the fluidic system was operated for 1 h before connecting the device to ensure the air was properly humidified. The device was connected to the rest of the fluidic system through the tubing connectors. Airflow was then applied for different durations and shear stresses. Samples were then either stained for cell viability, or fixed and prepared for immunofluorescence imaging. Detailed experimental timelines for each type of investigation and cell type are shown in Tables I–III.

TABLE I. Experimental timeline for exposing BEAS-2B cells to airflow shear stresses to investigate cytoskeletal organization or cell viability.

Day 0	Day 0+3 h	Day 2	Day 8	Day 9
Seed cells in 80 μl droplet	Submerged liquid culture	Cells 100% confluent, induce air-liquid interface	Apply airflow for 2, 12, 24 H at 0.5 dynes/cm^2	Fix and prepare for immunofluorescence imaging

TABLE II. Experimental timeline for exposing HTEC cells to airflow shear stresses to investigate cytoskeletal organization or cell viability.

Day 0	Day 0 +3 h	Day 7	Day 11	Day 12
Seed cells in 80 μl droplet, droplet composed of B-ALI media, without B-ALI inducer	Cells 90% Confluent, induce air-liquid interface with B-ALI Media and B-ALI inducer	Cells 100% Confluent	Apply airflow for 24 H at 0.5 dynes/cm^2	Fix and prepare for immunofluorescence imaging of airflow exposed and static samples

TABLE III. Experimental timeline for exposing HTEC cells to airflow shear stresses to investigate cilia beating orientation.

Day 0	Day 0+3 h	Day 7	Day 14–17	Day 24	Day 26–35	Day 38
Seed cells in 80 μl, droplet composed of B-ALI media, without B-ALI inducer	Cells 90% confluent, induce air-liquid interface with B-ALI media and B-ALI inducer	Cells 100% confluent	Cilia start to appear, seen using 40× objective lens	Apply airflow for 24 H at 0.5 dynes/cm^2	Elongated cilia can been using 10× objective lens, high mucociliary transport observed	Ciliary beating assay, fix and prepare for immunofluorescence imaging of airflow exposed and static samples

F. Staining

To process the samples, media in the basal chamber was removed and the devices were dissected by cutting out the device from the filter membrane insert and separating the lid layer from the frame layer; this leaves the membrane and the frame layer for easier analysis. Samples for immunocytochemical staining were then rinsed with PBS, fixed with 4% paraformaldehyde for 10 min, permeabilized with 0.1% Triton X-100 in PBS for 20 min and stained. Microtubules were stained with a mouse monoclonal anti-β-tubulin primary antibody (Abcam, ab7792) at a dilution of 1:200 and Goat anti-mouse Alexa Fluor 488 secondary antibody (Invitrogen). F-actin was stained using rhodamine conjugated phalloidin (Invitrogen) at a dilution of 1:100 in PBS. Nuclei were stained using 0.5 μg/ml of 4′, 6-diamidino-2-phenylindole (DAPI). Cilia were visualized using a monoclonal anti-acetylated α-tubulin (T7451, Sigma) at a dilution of 1:200. Cell viability was quantified by staining samples with Calcein AM for viable cells and Ethidium Homodimer-1 for non-viable cells using a Live/Dead Viability Assay (Invitrogen).

G. Microscopy

For low magnification images, the entire apical slot was imaged using a fluorescence inverted microscope (Olympus IX81 with X-Cite Series 120PC Q illumination source) in a raster scan with a 10× objective lens using the Scan Slide function of the microscopy software (Metamorph Premier). For high magnification imaging, filter membranes were cut out from the slot, mounted on a glass slide (GoldLine Microscope Slides, VWR) and imaged with a fluorescence laser confocal microscope (FV1000 Olympus IX81) at three positions in the centre of the channel where the highest amount of shear stress was located as determined by the CFD model. At these positions, Z-stack image slices were taken for the entire monolayer with 0.6 μm between slices to form a three dimensional image.

H. Quantification of fibre orientation

Images were processed with FIJI software. Separate images of the basal and apical f-actin sections of the slides were created by taking a maximum intensity Z-projection of the first and last 30% of the en-face Z-stack slides, respectively. Microtubule images were created by taking a maximum intensity Z-projection of the entire Z-stack. The Z-projected images were pre-processed for fibre orientation by applying a Gaussian blur of 1 pixel to remove speckled noise in the images. Fibre orientation was determined using the OrientationJ Distribution plug-in for FIJI.[28]

I. Ciliary beating assay

Apical surfaces of samples were washed twice with culture medium for 10 min to remove mucous from the monolayer. After washing, 23 μl of medium containing 0.5 μm yellow-green fluorescent microspheres (FluoSpheres® Carboxylate-Modified Microspheres, Life Technologies) at a 1:1000 concentration was added to the apical slot, and 1 ml of medium was added to the basal chamber. Note the culture medium used here was Minimal Essential Medium (MEM), 1% 100× MEM Non-Essential Amino Acids (GIBCO), 20% FBS and 1% penicillin/streptomycin. Culture dishes were placed in a live cell chamber set at 37 °C (LQ live cell instrument CU-109) and the beads were imaged using a fluorescent inverted microscope (Olympus IX81 with X-Cite Series 120PC Q illumination source). Videos of the fluorescent beads were created by taking 100 images at 11 frames per second with an exposure time of 35 ms per image. Ciliary beating was visually verified by taking phase-contrast and fluorescent microscopy videos of ciliated cells. Videos of the entire apical surface were taken by performing a raster scan of the sample.

Videos were processed by removing non-moving particles through a minimum Z-projection subtraction algorithm. Tracks of bead movement were generated by producing a maximum Z-projection of the image stack to visualize ciliary beating streamlines and stitched together using the Grid/Collection Stitching plug-in for FIJI[29] to create a complete image of the whole cell monolayer. Stitched ciliary beating streamlines and acetylated α-tubulin images were overlaid on top of each other using graphics editing software (Adobe Photoshop Elements 9, Adobe Systems) through a linear addition overlay. The orientation of the ciliary beating was then determined manually by watching each video and drawing an arrow parallel and on top of the bead streamlines using graphics editing software (Adobe Photoshop Elements 9, Adobe Systems). Individual bead movement was tracked using the TrackMate plug-in for FIJI and velocities of the beads were determined using the TrackMate analysis function. Tracks are characterized into areas with significant fluidic transport and minimal fluidic transport. Areas with significant fluidic transport are characterized as regions with velocities greater than 20 μm/s and having bead track lengths (stream lengths) longer than 300 μm and adjacent beads tracks being parallel (stream widths) within a 150 μm region.

III. RESULTS AND DISCUSSION

A. Device design

A novel custom built fluidic device was designed and fabricated to culture airway epithelial cells at the air liquid interface while incorporating a fluidic channel to apply airflow over the cells (Figure 1(a)). The device was designed to fulfill certain requirements: enable cell culture in an air-liquid interface configuration, allow application of controlled airflow shear stresses for 24 h, and be compatible with conventional imaging techniques. In addition, we wanted the device to be easy to operate to encourage wide-spread use.

The fluidic device has a modular assembly made from a combination of polystyrene and adhesive components designed to be incorporated into a 6-well filter membrane insert. The device is comprised of a polystyrene slotted disc (known as the frame layer), where cells are cultured, and a top polystyrene lid (known as the lid layer). The slot in the frame layer functions

as an open channel and is attached to a porous polyester membrane using a silicone adhesive transfer tape. The open channel generated by the frame layer was designed to be a backwards forward facing step with a step height of 0.4 mm (Figure 1(a)). The purpose of the step in the design was to protect cells from incoming air that would directly impact the cells at the 90° angle bend. The lid layer is adhered on top of the frame layer using a polyacrylic adhesive transfer tape to create an enclosed fluidic channel. Perfusion of fluids through the fluidic channel is possible through the inlet and outlet connectors housed in the lid layer.

Our device design was the result of an extensive refinement process with adhesion between the layers to prevent leakage being a dominant factor. Initially, polydimethylsiloxane (PDMS) was used to fabricate the frame and lid layers. In initial testing, it was found that it was difficult to adhesively bond the polyester membrane and PDMS layers. This unsatisfactory bond led to continual leakages and the system was not robust enough for reliable use. Instead polystyrene was chosen for its mechanical properties (more rigid than PDMS), cytocompatibility, gas impermeability, and higher surface energy that allowed stronger bonds to adhesives.[30] We also tested a number of adhesive transfer tapes with the final selection based upon cytocompatibility, thickness, substrate compatibility, and strength. Several poly-acrylic and silicone based adhesive transfer tapes were tested; the polyacrylic adhesive transfer tape was selected for bonding the frame layer to the lid layer due to its strong bonding capabilities and cytocompatibility. For the adhesive bond between the frame layer and the porous filter membrane, a silicone adhesive transfer tape was selected because of the adhesive's 1 mil thickness, cytocompatibility, and excellent bonding properties between the polyester membrane and to the polystyrene frame layer.

The final device design and fabrication protocol is an easy to operate system with low-start-up costs that can be adopted easily by other laboratories, as the microfabrication does not rely on lithography techniques that require a clean room. The prominent feature of the fluidic device is that cells can be seeded into an apical open slot and this slot can be enclosed at a later time for perfusion of fluids in the apical chamber. The perfusion of fluids through the apical channel allows the application of airflow shear stresses on airway epithelial cells at any chosen time point in the differentiation process. Furthermore, our device incorporates standard filter membrane inserts, the gold standard surface for epithelial cell culture, and because the cells are seeded directly on the apical slot, the user has more control over cell density and the location of where the cells attach than in a pre-formed device where the cells are enclosed in channels during the seeding process.

B. Air flow circuit design and characterization

The fluidic system is comprised of three sub-systems: an airflow conditioning system, the fluidic device containing the cells, and a data acquisition system that monitors the airflow rates being applied. An overview of the components and operation of the fluidic system is shown in Figure 1(b). The purpose of the airflow conditioning system was to sterilize and maintain the humidity and temperature of the air at 95%+ relative humidity and 37 °C. To assess leakage in the device, we measured the airflow at the inlet and outlet at different flow rates (Figure 2(a)). Over the range of flow rates tested, we did not observe leakage within the system: measurements at the inlet and outlet were the same within the accuracy of the air flow sensors. Limiting any possible leakage was important to ensure accurate and sustained levels of shear stress could be applied to the cells within the device.

To assess the variation in shear stress levels within our device and confirm the device operates within the physiological levels specified in our design criteria, we developed a computational fluid dynamic model to describe air flow patterns and the corresponding shear stress patterns within our device. We calculated a Reynolds number of 70 suggesting laminar flow could be assumed within the device when using a flow rate of 0.17 l/min. The CFD model showed unidirectional airflow from the inlet to the outlet (Figure 2(b)). The device was sized to resemble flow rates and Reynolds numbers thought to be in the first few generations of the respiratory system where tidal breathing or light breathing is modelled to have a Reynolds number of

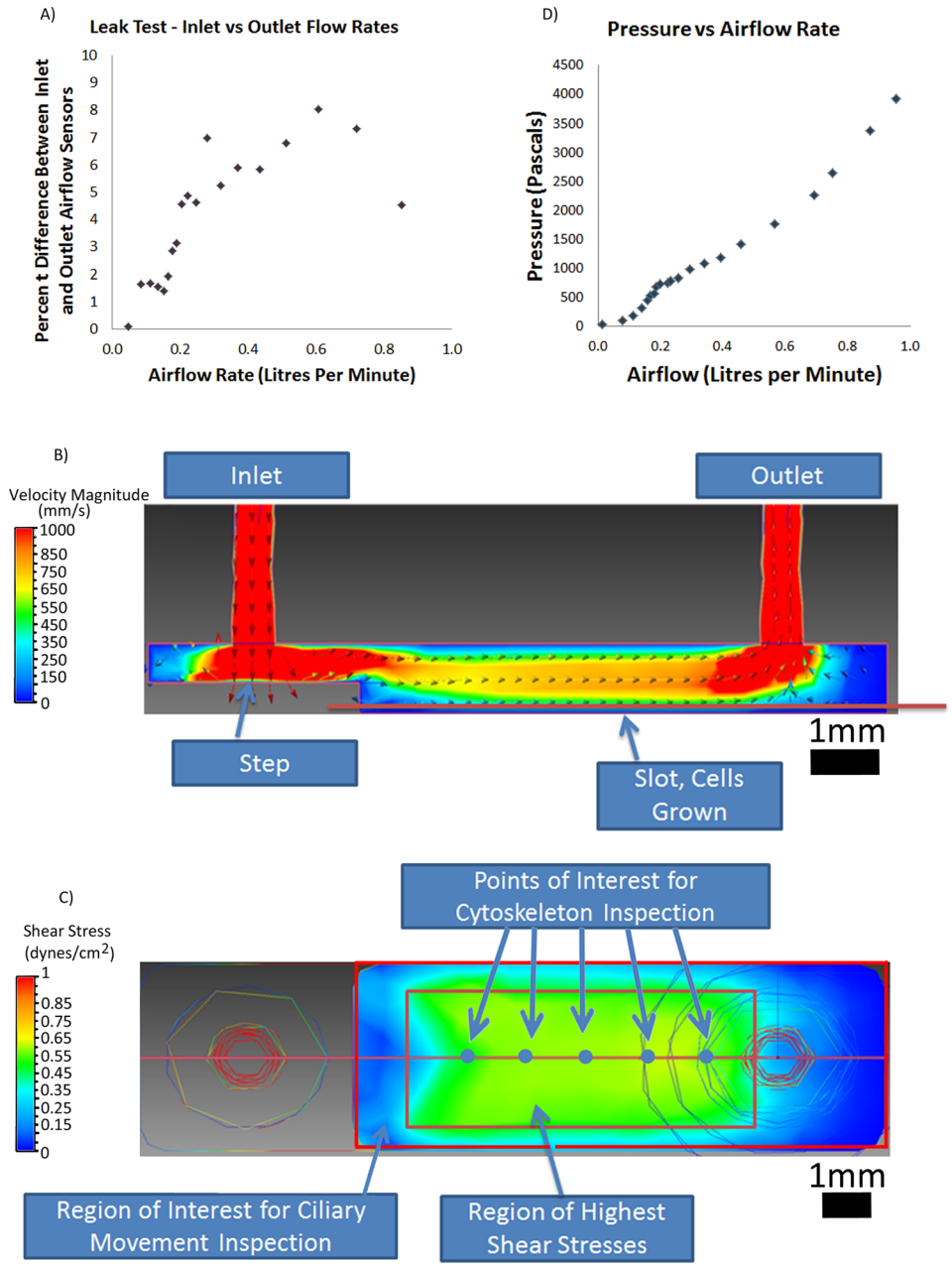

FIG. 2. System flow characteristics. (a) Plot of system leakage as a function of flow rate. (b) Computational model of flow rate within the device. (c) Calculated shear profile on surface of cells within the device. (d) Channel pressure drop as a function of flow rate.

approximately 90 and an approximate air flow rate of 0.157 l/s.[31,32] In the model, the highest rate of airflow was in the connecting tubes. The model also suggests that the step feature in our design did absorb the impact of the airflow.

Since the region near the backward facing step has airflow rate dependant recirculating zones, cells seeded near the step were considered inappropriate for taking measurements. From our airflow model, we estimated the shear stress variation on the membrane region of our device where the cells are located (Figure 2(c)). The region of highest shear is uniform within a range of 0.5 mm from the wall and is rectangular in shape. For this reason, we decided to assess cell behaviour in the central region where shear was uniform (green region in Figure 2(c)). The

flow rate in this region corresponded to a shear level of 0.5 dynes/cm^2, which physiologically corresponds to a person engaged in a low-intensity activity or resting.[31,32] This confirmed that air flow rates corresponding to physiologically relevant shear levels found in generation 0 to generation 5 branches of the respiratory tree were possible using the device.[26,32,33] Furthermore, to assess whether our system operated within physiologically relevant pressure ranges, we also measured pressure drop across the device as a function of flow rate (Figures 2(d)). For flow rates corresponding to shear stresses between 0 and 4 dynes/cm^2, we measured pressures between 0 and 4 kPa. This corresponded to our physiological target range suggesting that pressure in the device was appropriate as trans-airway pressures in the respiratory tree can reach 0.9 kPa and alveolar pressures can reach 4.0 kPa during breathing.[34]

C. Cell viability and function

We first assessed BEAS2B cell viability in our device under both static and air flow conditions. Humidification control in the system was critical. Cells exposed to airflow without the air conditioning system were only viable for 6 h, with complete cell monolayer death occurring after 12 h of airflow (Figure 3(b) and data not shown). With the air conditioning sub-system connected and operating, cells were viable for a period of at least 24 h of airflow stimulation (Figure 3(c)). Extended periods of stimulation, longer than 24 h, were not tested and left for future studies.

We next set out to assess if primary cells could remain viable and apically-basally polarize and form cilia within our device. We found that primary HTEC differentiated and formed motile cilia, similar to what is observed in a standard Transwell (Figure 3(d)), when cultured in the device over a period of 38 days at air-liquid interface culture without (Figure 3(e)) and with airflow (Figure 3(f)). In both airflow and static samples, patches of multiciliated cells could be seen with functioning beating cilia that were able to produce significant amounts of ciliary transport and are compared to standard Transwell culture (movies 1–9 in the supplementary material).[43] Furthermore, applying 24 h of airflow at 0.5 dynes/cm^2 during the maturation process (day 24 of air-liquid interface culture) resulted in the same number of cilia formed after 38 days of air-liquid interface culture. Specifically, we measured a mean density of 969 ± 118

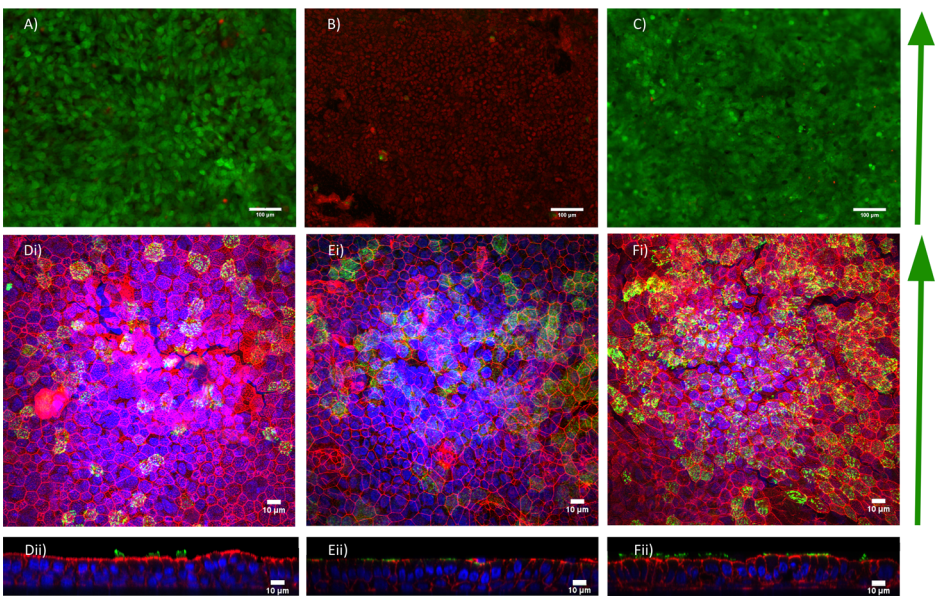

FIG. 3. (a)–(c) Cell viability and functionality of BEAS-2B cells. (a) Cell viability in static case, (b) flow without humidification and (c) flow with humidification conditions after 24 h. Red indicates dead cells and green indicates live cells. (d)–(f) Human tracheal epithelial cells after 38 days of culture on (d) standard transwell inserts, (e) in the device without application of flow, and (f) with flow applied at day 24 for 24 h. (di–fi) Enface images (dii–fii) cross-sectional Z-stack images, red = phalloidin (F-actin), Green = acetylated α-tubulin (cilia), blue = DAPI (nuclei).

ciliated cells/mm^2 ($\pm$standard error of mean (SEM)) in static standard filter membrane inserts, while in the device we measured a mean density $1216 + 23.6$ (SEM) ciliated cells/mm^2 and $1223 + 86$ (SEM) ciliated cells/mm^2 in the airflow cases. These results suggested that cells could apicobasally polarize and differentiate into ciliated cells normally in our system when comparing to standard Transwell culture.

D. Capacity to quantify epithelium organization in our device

We next set out to demonstrate the compatibility of our device with standard techniques to assess epithelial organization. An important metric to quantify epithelium organization is cytoskeletal organization. We therefore assessed apical actin organization and microtubules in cells exposed to airflow at 0.5 dynes/cm^2 air flow for 24 h and without airflow in both BEAS-2B (Figure 4) and HTEC (data not shown). As expected, BEAS-2B cells formed confluent stratified layers in a squamous cell shape. In contrast, HTEC formed confluent pseudostratified monolayers in a columnar cell shape which is similar to *in vivo* where cells appear to be stratified but rather are all in contact with the basal surface. Both actin and microtubule fibres could be easily imaged in our system (Figure 4), highlighting the benefit of our system design that allows disassembly for sample analysis. This is particularly important for cells being grown on Transwell cultures, as the surface of the cells must be assessable for sufficient image quality for automated quantitative analysis to be conducted. Indeed automated analysis of our images was possible (Figure 4).

Another important metric that is particularly useful for characterizing the organization and function of airway epithelium is the orientation of cilia beating. A standard method to quantify cilia beat direction is the bead flow assay in which micrometre sized fluorescence beads are placed in a liquid solution on top of the cilia[11,13,15] and their motion tracked using high speed microscopy, allowing the direction of cilia beating to be determined. We therefore set out to conduct this assay in our system on cells exposed to both static and air flow conditions. In both the airflow and static cases in the device, there were areas of high ciliary transport throughout the channel that resulted in bead movement; similar to cells cultured on standard filter insert cultures but showing different macroscopic flow patterns (Figure 5, movies 1–9 in the supplementary material).[43] In all cases (standard Transwells, static and flow devices), only partial areas of ciliary movement were observed. This is because each ciliated cell can only produce enough force to propel the beads through the fluid a set distance due to viscous drag forces.

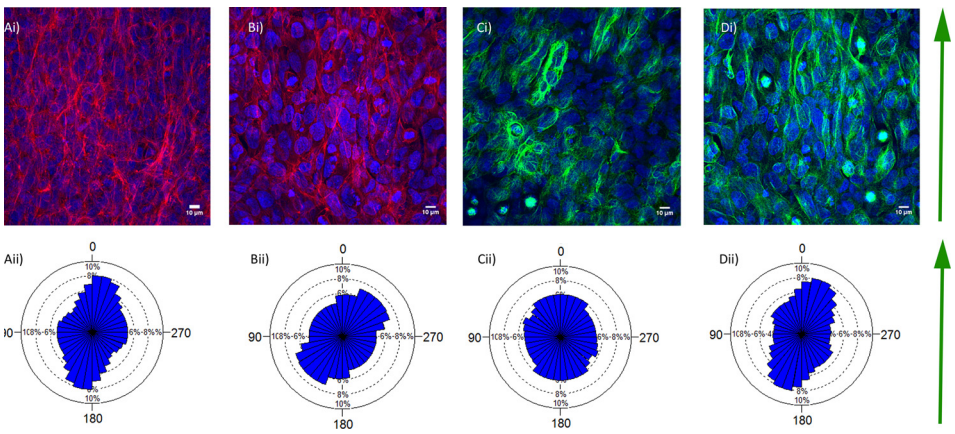

FIG. 4. Cytoskeletal response to airflow in BEAS2B cells. (a) Apical actin organization (stained with phalloidin) in BEAS2B cells at 24 under static conditions (ai) and corresponding rose plot showing fibre orientation (aii). (b) Apical actin organization (stained with phalloidin) in BEAS2B cells exposed to 0.5 dynes/cm^2 air flow for 24 h (bi) and corresponding rose plots showing fibre orientation (Bii). (c) Microtubule orientation shown by acetylated tubulin staining in static conditions (ci) and the corresponding rose plot of microtubule orientation (cii). (d) Microtubule orientation shown by acetylated tubulin staining in cells exposed to 0.5 dynes/cm^2 for 24 h (di) and the corresponding rose plot of microtubule orientation (dii). Red = phalloidin (F-actin), green = β-tubulin, blue = DAPI (nuclei).

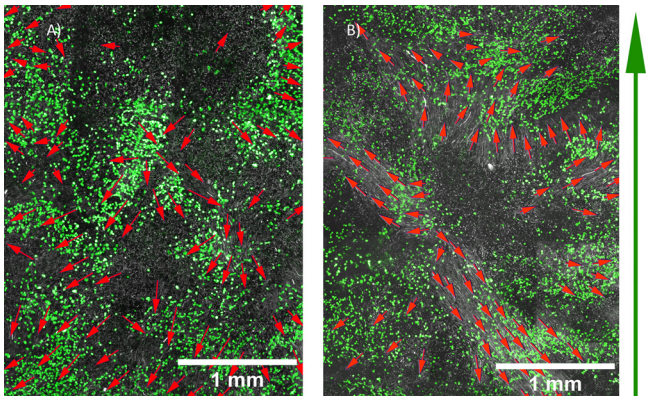

FIG. 5. Bead movement direction indicating cilia beat direction in HTEC after 38 days air-liquid interface culture under static conditions (a) and in cells exposed to 0.5 dynes/cm^2 for 24 h at 24 days air-liquid interface culture (b). White = fluorescent beads, green = acetylated α-tubulin (cilia), red arrows = beating direction, green arrow = airflow direction.

The force the ciliated cell can produce is dependent on the length of the cilia, with longer cilia being able to generate more fluidic transport and short cilia unable to generate significant fluidic transport. Partial areas of ciliary movement are therefore seen since only a certain percentage of cells at the apical surface differentiate into ciliated cells and only regions with ciliated cells are seen to create fluidic transport. Observations during video microscopy of the ciliated cells showed that the cilia sucked in beads from above the cell, propelled the bead forward, and then the bead floated back up. Interestingly, in both standard Transwell cultures and our device under both static and shear flow conditions, a layer of mucous covered the apical layer of the cells. Large mucous clumps are difficult to be moved by cilia and beads appear to twitch back and forth at high frequency if they become trapped in this mucous. Prior to the application of the beads, it was therefore important to wash away this mucous to avoid beads becoming trapped and aggregated and to ensure accurate quantification. The ability to disassembly our device for analysis was advantage for this purpose.

Bead movement could be tracked to determine cilia beat direction (Figure 5). Using our bead assay, the approximate range of bead velocities in a standard Transwell insert was 33 to 124 μm/s with a mean of 76 μm/s + 12.5 μm/s (SEM) in areas with significant fluidic transport, which is consistent with fluidic transport rates ranging from 40 to 92 μm/s[12] observed in other standard Transwell filter inserts studies.[26,35] The approximate range of bead velocities in the airflow system was 12 to 70 μm/s with a mean of 25 μm/s + 4.4 μm/s (SEM) in areas with significant fluidic transport, which is lower than but in the same range as our Transwell control. We speculate that this difference and the difference in flow patterns observed could arise from a number of factors that impact cilia behaviour and ability to move beads in this assay, such as differences in mucus production levels between our system and standard Transwells during culture or differences in the shape of standard Transwells versus our device that lead to differences in the local flow of mucus during ALI culture that impact cilia orientation. The factors that impact cilia beat velocity and flow patterns in this assay are complex and our system provides an interesting tool to study this further in the future.

Our device provides a robust system for exploring the impact of air flow on the organization and functionality of polarizing airway epithelium. In the future, it would be useful to expand our studies beyond 24 h to longer exposure times, potentially up to 38 days, the time for complete HTEC polarization to be completed. It is possible, however, that the application of air flow during the entire long maturation process is not necessary, as current studies suggest that a limited time window exists during which ciliary beat direction is defined. It is known that ciliogenesis and ciliary development occur in many sequential stages.[9,36] In the first stage, cells become confluent and start to apically basally polarize. As the cells polarize, microtubules become aligned within the cell and the planar cell polarity (PCP) proteins become asymmetrically distributed.[37] During the second stage, cells begin differentiating into multiciliated cells

during which the cell reproduces basal bodies[38,39] and the primary cilium within the cell disassembles and retracts to the apical surface.[40] In the third stage, the basal bodies dock to the subapical surface of the cell, attach to basal feet, and cilia elongate through the apical surface.[41] Basal bodies are then aligned by an organized microtubule network.[9] The fourth stage is a refinement stage in which the cilia are able to create small amounts of fluid flow and refine their beating direction in the same direction as the induced fluid flow in a positive feedback loop.[15] This refinement is able to override the initial PCP signalling controlling the rotational polarity of the cell.[14,15,42] The cilia then elongate further to become fully matured and at this final stage, ciliary orientation is permanently set and cannot be altered by fluidic shear stresses.[15] For example, in a study by Guirao *et al.*,[15] ciliated mouse ependymal cells exposed to external fluidic shear stresses of 0.018 dynes/cm^2 using a rotating plate system aligned ciliary beating in the direction of the fluidic stresses but only if forces were applied during the refinement phase when cilia were motile and elongating; as application of fluidic shear stresses before and after the refinement phase did not alter ciliary orientation. Mouse tracheal epithelial cells (mTEC) are known to start forming motile cilia after ∼4 days in air-liquid interface culture and then the percentage of cells containing cilia plateaus by days 10–12 after air-liquid interface culture.[40] Similarly, HTEC in our system begin showing cilia after ∼14 to 17 days of air-liquid interface culture and these elongate and begin beating with sufficient force to move a bead by 21 days of air-liquid interface culture, therefore future experiments will target application of 0.01–0.5 dynes/cm^2 flow during this time window (∼days 13 to 25) specifically when we predict cilia orientation is flow-responsive. The suggested shear flow rate range includes a wider range of flows that are much higher than those known to produce cilia alignment with liquid flow,[15] because the mucous layer secreted by the airway epithelial cells may protect the cells from airflow shear stresses by creating a sticky layer that is bound to cells and difficult to displace by airflow, thus reducing the shear stresses the cells experience. A further possible development to our system and protocols would be optimization of the disassembly process to enable subsequent re-assembly. This would enable periodic removal of the mucous layer. Furthermore, this would allow, for example, periodic assessment of cilia beat direction using the bead assay and other assays that require direct access to the cells, to be conducted at different time points during the polarization process.

IV. CONCLUSIONS

We have developed a fluidic system capable of exposing airway epithelial cells to controlled shear stresses at a variety of rates, durations, and time points with device features that makes the system easy to utilize. The platform developed is useful to investigate the effects of airflow shear stresses not only on epithelial organization but also on other functional parameters of airway epithelial cells, such as mucin secretion, airway surface liquid absorption, and epithelial barrier function. Utilizing the system, we determine that humidity plays a critical role in maintaining cell viability when exposing cells to long-term airflow stimulation and this crucial design feature should be incorporated in any future long-term airflow stimulation studies. Furthermore, primary HTEC in the device functionally differentiated into an epithelium containing ciliated cells. Our study also showcases the compatibility of our device with standard tools used to quantify epithelium organization such as cytoskeleton organization and cilia beat orientation. We envision our tool will be useful for designing future *in vitro* devices that recapitulate functioning epithelium by incorporating air-liquid interface culture.

ACKNOWLEDGMENTS

The authors wish to thank Dr. Nadeem Moghal for supplying the HTEC cells and Connie Rogers-Newcome of Adhesives Research Inc. for providing the silicone adhesive transfer tape. This work was funded by a National Science and Engineering Research Council (NSERC)/Canadian Institute of Health Research (CIHR) Collaborative Health Research Program Grant (No. CHRP 399494-2011) to A.P.M. and T.K.W., and Training Program in Regenerative Medicine/CIHR and NSERC graduate scholarships to D.T. The authors have no conflict of interests to declare.

[1]H. C. Grillo, Ann. Thorac. Surg. **75**, 1039 (2003).
[2]P. Jungebluth, E. Alici, S. Baiguera, K. Le Blanc, P. Blomberg, B. Bozoky, C. Crowley, O. Einarsson, K. H. Grinnemo, T. Gudbjartsson, S. Le Guyader, G. Henriksson, O. Hermanson, J. E. Juto, B. Leidner, T. Lilja, J. Liska, T. Luedde, V. Lundin, G. Moll, B. Nilsson, C. Roderburg, S. Stromblad, T. Sutlu, A. I. Teixeira, E. Watz, A. Seifalian, and P. Macchiarini, Lancet **378**, 1997 (2011).
[3]P. Macchiarini, T. Walles, C. Biancosino, and H. Mertsching, J. Thorac. Cardiovasc. Surg. **128**, 638 (2004).
[4]P. Macchiarini, P. Jungebluth, T. Go, M. A. Asnaghi, L. E. Rees, T. A. Cogan, A. Dodson, J. Martorell, S. Bellini, P. P. Parnigotto, S. C. Dickinson, A. P. Hollander, S. Mantero, M. T. Conconi, and M. A. Birchall, Lancet **372**, 2023 (2008).
[5]M. J. Elliott, P. De Coppi, S. Speggiorin, D. Roebuck, C. R. Butler, E. Samuel, C. Crowley, C. McLaren, A. Fierens, D. Vondrys, L. Cochrane, C. Jephson, S. Janes, N. J. Beaumont, T. Cogan, A. Bader, A. M. Seifalian, J. J. Hsuan, M. W. Lowdell, and M. A. Birchall, Lancet **380**, 994 (2012).
[6]X. Luo, Y. Liu, Z. Zhang, R. Tao, Y. Liu, A. He, Z. Yin, D. Li, W. Zhang, W. Liu, Y. Cao, and G. Zhou, Biomaterials **34**, 3336 (2013).
[7]D. St. Johnston and J. Ahringer, Cell **141**, 757 (2010).
[8]M. E. Werner, P. Hwang, F. Huisman, P. Taborek, C. C. Yu, and B. J. Mitchell, J. Cell Biol. **195**, 19 (2011).
[9]E. K. Vladar, R. D. Bayly, A. M. Sangoram, M. P. Scott, and J. D. Axelrod, Curr. Biol. **22**, 2203 (2012).
[10]P. H. Karp, T. O. Moninger, S. P. Weber, T. S. Nesselhauf, J. L. Launspach, J. Zabner, and M. J. Welsh, Methods Mol. Biol. **188**, 115 (2002).
[11]H. Matsui, S. H. Randell, S. W. Peretti, C. W. Davis, and R. C. Boucher, J. Clin. Invest. **102**, 1125 (1998).
[12]A. L. Oldenburg, R. K. Chhetri, D. B. Hill, and B. Button, Biomed. Opt. Express **3**, 1978 (2012).
[13]B. Button, M. Picher, and R. C. Boucher, J. Physiol. **580**, 577 (2007).
[14]B. Mitchell, R. Jacobs, J. Li, S. Chien, and C. Kintner, Nature **447**, 97 (2007).
[15]B. Guirao, A. Meunier, S. Mortaud, A. Aguilar, J. M. Corsi, L. Strehl, Y. Hirota, A. Desoeuvre, C. Boutin, Y. G. Han, Z. Mirzadeh, H. Cremer, M. Montcouquiol, K. Sawamoto, and N. Spassky, Nat. Cell Biol. **12**, 341 (2010).
[16]L. E. Ostrowski and P. Nettesheim, Express Lung Res. **21**, 957 (1995).
[17]N. Even-Tzur, Y. Kloog, M. Wolf, and D. Elad, Biophys. J. **95**, 2998 (2008).
[18]N. E. Davidovich, Y. Kloog, M. Wolf, and D. Elad, Biophys. J. **100**, 2855 (2011).
[19]C. F. Chen, J. Liu, L. P. Hromada, C. W. Tsao, C. C. Chang, and D. L. DeVoe, Lab. Chip **9**, 50 (2009).
[20]E. W. Young, A. R. Wheeler, and C. A. Simmons, Lab. Chip **7**, 1759 (2007).
[21]C. E. Stewart, E. E. Torr, N. H. Mohd Jamili, C. Bosquillon, and I. Sayers, J. Allergy (Cairo) **2012**, 943982.
[22]R. R. Reddel, Y. Ke, B. I. Gerwin, M. G. McMenamin, J. F. Lechner, R. T. Su, D. E. Brash, J. B. Park, J. S. Rhim, and C. C. Harris, Cancer Res. **48**, 1904 (1988).
[23]J. H. Widdicombe, L. A. Sachs, J. L. Morrow, and W. E. Finkbeiner, BioTechniques **39**, 249 (2005).
[24]A. Dvorak, A. E. Tilley, R. Shaykhiev, R. Wang, and R. G. Crystal, Am. J. Respir. Cell Mol. Biol. **44**, 465 (2011).
[25]J. R. Rock, M. W. Onaitis, E. L. Rawlins, Y. Lu, C. P. Clark, Y. Xue, S. H. Randell, and B. L. Hogan, Proc. Natl. Acad. Sci. U.S.A. **106**, 12771 (2009).
[26]R. Tarran, B. Button, M. Picher, A. M. Paradiso, C. M. Ribeiro, E. R. Lazarowski, L. Zhang, P. L. Collins, R. J. Pickles, J. J. Fredberg, and R. C. Boucher, J. Biol. Chem. **280**, 35751 (2005).
[27]R. Tarran, Proc. Am. Thorac. Soc. **1**, 42 (2004).
[28]R. Rezakhaniha, A. Agianniotis, J. T. Schrauwen, A. Griffa, D. Sage, C. V. Bouten, F. N. van de Vosse, M. Unser, and N. Stergiopulos, Biomech. Model. Mechanobiol. **11**, 461 (2012).
[29]S. Preibisch, S. Saalfeld, and P. Tomancak, Bioinformatics **25**, 1463 (2009).
[30]E. Berthier, E. W. Young, and D. Beebe, Lab Chip **12**, 1224 (2012).
[31]U.S. EPA, *Metabolically Derived Human Ventilation Rates: A Revised Approach Based Upon Oxygen Consumption Rates (Final Report)* (U.S. Environmental Protection Agency, Washington, DC, 2009).
[32]G. Xia, M. H. Tawhai, E. A. Hoffman, and C. L. Lin, Ann. Biomed. Eng. **38**, 1836 (2010).
[33]C. L. Lin, M. H. Tawhai, G. McLennan, and E. A. Hoffman, Respir. Physiol. Neurobiol. **157**, 295 (2007).
[34]R. Rhoades and D. R. Bell, *Medical Physiology: Principles for Clinical Medicine* (Lippincott Williams & Wilkins, Baltimore, MD, USA, 2013), pp. 350–353.
[35]B. Button, R. C. Boucher, and University of North Carolina Virtual Lung Group, Respir. Physiol. Neurobiol. **163**, 189 (2008).
[36]M. E. Werner and B. J. Mitchell, Curr. Biol. **22**, R1001 (2012).
[37]E. K. Vladar and J. D. Axelrod, Trends Cell Biol. **18**, 517 (2008).
[38]E. K. Vladar and T. Stearns, J. Cell Biol. **178**, 31 (2007).
[39]F. E. Tan, E. K. Vladar, L. Ma, L. C. Fuentealba, R. Hoh, F. H. Espinoza, J. D. Axelrod, A. Alvarez-Buylla, T. Stearns, C. Kintner, and M. A. Krasnow, Development **140**, 4277 (2013).
[40]R. Jain, J. Pan, J. A. Driscoll, J. W. Wisner, T. Huang, S. P. Gunsten, Y. You, and S. L. Brody, Am. J. Respir. Cell Mol. Biol. **43**, 731 (2010).
[41]E. K. Vladar and S. L. Brody, Methods Enzymol. **525**, 285 (2013).
[42]Y. H. Chien, M. E. Werner, J. Stubbs, M. S. Joens, J. Li, S. Chien, J. A. Fitzpatrick, B. J. Mitchell, and C. Kintner, Development **140**, 3468 (2013).
[43]See supplementary material at http://dx.doi.org/10.1063/1.4901930 for computational fluid dynamics inlet boundary condition and ciliary beating assay movies for human tracheal epithelial cells.